Chemical Science

MINIREVIEW

View Article Online
View Journal | View Issue

Cite this: *Chem. Sci.*, 2018, **9**, 4546

Electrochemical imaging of cells and tissues

Tzu-En Lin,[a] Stefania Rapino,[b] Hubert H. Girault[a] and Andreas Lesch*[a]

Received 4th March 2018
Accepted 9th April 2018

DOI: 10.1039/c8sc01035h

rsc.li/chemical-science

The technological and experimental progress in electrochemical imaging of biological specimens is discussed with a view on potential applications for skin cancer diagnostics, reproductive medicine and microbial testing. The electrochemical analysis of single cell activity inside cell cultures, 3D cellular aggregates and microtissues is based on the selective detection of electroactive species involved in biological functions. Electrochemical imaging strategies, based on nano/micrometric probes scanning over the sample and sensor array chips, respectively, can be made sensitive and selective without being affected by optical interference as many other microscopy techniques. The recent developments in microfabrication, electronics and cell culturing/tissue engineering have evolved in affordable and fast-sampling electrochemical imaging platforms. We believe that the topics discussed herein demonstrate the applicability of electrochemical imaging devices in many areas related to cellular functions.

Introduction

A broad range of analytical tools has been developed to image biological functions *in vivo* and *in vitro* with the major goal being to provide a better understanding of biological processes and to improve diagnostics and therapies. Optical detection methods, such as fluorescence microscopy, are standard for imaging *in vitro* samples, as these methods are fast and do not require specific sample preparation steps apart from excising/culturing and tagging. Tomographic bio-imaging techniques based on radioactive labels are used for *in vivo* analysis, but are generally limited in spatial resolution. Mass spectrometry imaging is widely used for visualizing biomarker distributions but has limitations when applied for quantification. Electrochemical platforms are attractive due to their ability to detect electroactive species in solution by an electron transfer reaction between a dissolved target compound and the electrode without suffering from optical interference from sample turbidity or auto-fluorescence. Quantification can be realized by the dependence of the recorded current on the analyte concentration. The range of detectable species is large, and specificity can be increased by addressing enzymatic activity with biosensing layers. Electrochemical methods for imaging have been available for nearly four decades, but they were mostly used for fundamental studies and technological developments. (Sub) micrometer-sized electrodes are typically applied, because they record diffusion-controlled steady-state currents as a result of a hemispherical diffusion field of the electroactive species at the electrode surface, which is an essential characteristic when translating the electrode for a certain amount of time over a specimen. Further advantages stem from fast response times, high signal-to-noise-ratio, low *iR*-drop and small capacitive charging currents. Advances in microfabrication and electronics have emerged now as platforms suitable for diagnostic imaging as a complementary technique or low-cost replacement of conventional bio-imaging. Herein, we shall give an overview about the progress that has been made in electrochemical imaging of live cells and hierarchical cell organizations, by emphasizing in particular the analysis of tissues. Physiological recordings and the detection of neurotransmitters in brain are well summarized in reviews related to neuroscience and are not part of this review. Single cells are suitable for fundamental studies, whereas 3D cell aggregates resemble *in vivo* situations more closely in terms of cell–cell interactions, cell–extracellular matrix interactions, and cell migration, differentiation, survival and growth. Biopsied tissues are interesting for diagnostics. In histopathology, thin tissue slices of <20 μm thickness ensure precise focusing, avoid strong scattering from irregular surfaces and enable the penetration of light throughout the entire tissue. However, ultrathin tissue sectioning may induce artifacts while thick tissue sections or even organs show nearly intact textures with a well-preserved cellular architecture. Thick tissue sections with a rugged surface are difficult to be observed under an optical microscope, and we will conclude this review with a view on promising electrochemical imaging applications for thick tissue analyses.

Electrochemical imaging techniques

Platforms for electrochemical imaging can be divided into two groups: (1) the biological sample is scanned with a nano- or micro-metric probe (often denoted as tip) recording data at

[a]*Laboratory of Physical and Analytical Electrochemistry (LEPA), École Polytechnique Fédéderale de Lausanne, EPFL Valais Valais, Rue de l'Industrie 17, CP 440, 1951 Sion, Switzerland. E-mail: andreas.lesch@epfl.ch*

[b]*Chemistry Department "Giacomo Ciamician", University of Bologna, Via Selmi 2, 40126 Bologna, Italy*

defined raster points and (2) the biological sample is deposited onto a microchip containing an array of individually addressable microelectrodes (MEs). The step size of the scanning probe and the separation between electrodes on the chip determine the electrochemical imaging resolution together with the electrode size, the substrate-to-sensor distance and the electrochemical detection strategy. The active electrode part and the sample are not in direct mechanical contact, and an electroactive species diffuses in solution between the sample and the electrode. The implementation of sensing devices on an optical microscope stage enables accurate probe positioning and complementary optical detection methods.

Electrochemical scanning probe microscopies (SPMs)

Scanning electrochemical microscopy (SECM)[1] and scanning ion conductance microscopy (SICM)[2] have emerged as powerful electrochemical imaging platforms. They are described in the following text with few exemplary operation principles, whereas imaging applications will be discussed later. SECM tips are usually based on Pt, Au or carbon disk electrodes of diameters below 25 μm down to the nanoscale surrounded by an insulating sheath.[3] In the feedback (FB) mode (Fig. 1a),[4] an

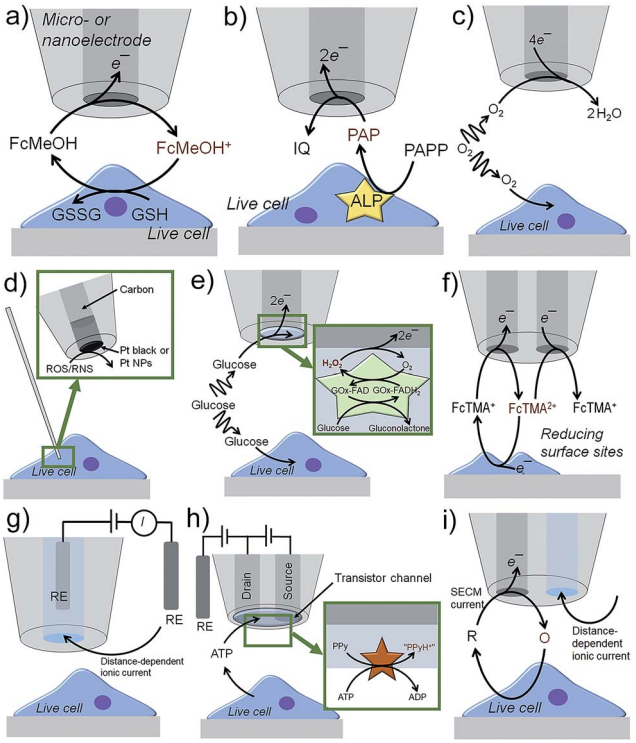

Fig. 1 Operation principles of typical electrochemical SPMs. (a) SECM feedback (FB) mode. (b) SECM substrate generation/tip collection (SG/TC) mode. (c) SECM redox (RC) competition mode. (d) Pt-Based nanoelectrode for non-invasive intracellular recordings. (e) Microbiosensor for specific metabolite detection. (f) Dual electrode SECM tip. (g) SICM for topographic mapping. (h) Nano-FET for specific metabolite detection. (i) SECM-SICM for constant distance mode electrochemical imaging. Please note that all schemes are not true to scale. Species written in brown color code were generated during the analysis for electrochemical detection.

electroactive species, *i.e.* a redox mediator like ferrocene methanol (FcMeOH), is present in solution and electrochemically oxidized at the SECM tip. The oxidized form of FcMeOH diffuses to the substrate, which is positioned within few tip radii away from the metal disk. Reactive sites in the sample, *e.g.* reducing molecules like glutathione (GSH), reduce the oxidized form of FcMeOH generating an additional flux of FcMeOH to the tip and thus enhancing the SECM current. Inactive surfaces block the diffusion of FcMeOH to the SECM tip resulting in a lower current.

The enzymatic activity of cellular structures can be analyzed by detecting their reactants or products, in case they are electroactive. Immunoassays, as they are used for enzyme-linked immunosorbent assays (ELISAs), can be adapted to target antigens. A primary antibody links to the target followed by linking a secondary antibody labeled with a specific enzyme that is known to generate or consume electroactive species. Examples are *p*-aminophenyl phosphate (PAPP) for alkaline phosphatase (ALP), hydrogen peroxide (H_2O_2) for glucose oxidase (GOx), *p*-aminophenyl-β-D-galactopyranoside (PAPG) for galactosidase and ferrocene derivatives for horseradish peroxidase (HRP).[5–8] The electroactive species can cycle between the enzyme and tip in the FB mode. Alternatively, the SECM tip can detect the flux of electroactive species initially not present, being the product of an enzymatic reaction at the substrate (substrate generation/tip collection (SG/TC) mode, Fig. 1b) and has the advantage over FB mode in that background currents are effectively zero. The SG/TC mode is limited to small sample areas and/or low enzymatic activity, because high and dense activity will result in semi-infinite, linearly growing diffusion profiles of the analyte lowering the experimental resolution over time. Pt MEs can be used to detect dissolved O_2 and to study the respiratory activity of live cells by letting the cell and the SECM probe compete for O_2 (redox-competition (RC), Fig. 1c).[9] Lower O_2 reduction currents at the SECM tip indicate the high respiratory activity of the cell as the cell consumes the O_2 in the electrolyte compartment under the SECM tip. Reactive oxygen and nitrogen species (ROS and RNS) play an important role in intracellular signaling, but can also cause oxidative stress, which potentially damages DNA and proteins. The electrochemical detection of ROS and RNS requires suitable electrocatalytic electrode materials, *e.g.* Pt black or platinized electrode surfaces.[10] The outer diameter of the tips must be in the nanometer range so that the tip can penetrate the cell membrane while preserving all cellular functions (Fig. 1d).[11,12] In order to detect specific metabolic analytes, such as glucose, lactate, D-serine or insulin, biosensing amperometric tips were introduced by depositing enzyme-containing matrices onto the active electrode surface.[13–16] The metabolites diffuse into the biosensing layer where they induce the enzymatic production of electroactive species, such as hydrogen peroxide (Fig. 1e). Potentiometric probes contain ion-selective layers to record the open circuit potential against a reference electrode as a response to changes in the concentration of ionic analytes, such as Ca^{2+}.[17] Individually addressable dual nano/microelectrodes use one electrode to oxidize an electroactive species, *e.g.* ferrocenylmethyl trimethylammonium ($FcTMA^+$),

and the second electrode to collect the oxidation product ($FcTMA^{2+}$, Fig. 1f).[18] Depending on the local reactivity of a nearby sample, *e.g.* a biologically induced reducing environment for $FcTMA^{2+}$, the generation and collection currents are enhanced and reduced, respectively. This enables local redox titrations[19] and potentially the investigation of molecular fluxes at the surface of cells: the first electrode would generate a species that the other electrode collects after it has interacted with cell functions.

Nanopipettes filled with an electrolyte solution are powerful probes for topographic imaging (Fig. 1g).[20] In SICM, an ionic current is driven by an electric field generated between an internal and external quasi-reference counter electrode (QRCE). The resistance between the two QRCEs increases inversely with the gap between the nanopipette and sample. The tip-to-substrate distance can be kept constant by setting the ionic current to a fixed value and implementing a feedback system for vertical nanopipette positioning.[20,21] By periodically modulating the voltage between the two QRCEs, the mass transport of ions into and out of the nanopipette can be controlled, a process that is further influenced by the charge of the surface of the nanopipette (typically glass) and by substrate charges. These effects can be used to extract the local surface charge of biological specimens from the measured properties of the diffuse double layer at a live cell–electrolyte interface.[22] Recently, nanopipettes were functionalized with glucose oxidase or with the pH-sensitive polymer chitosan for intracellular glucose or pH monitoring, respectively.[23,24] The ionic current changed due to charging effects in the sensing layers near the nanopipette orifice. Biosensing nanometric field-effect transistors (nano-FET) were produced by first filling the two channels of a double-barrel nanopipette with pyrolytic carbon as source and drain nanoelectrodes and second by coating the top of both electrodes with a layer of polypyrrole (PPy), which forms a transistor channel (Fig. 1h).[25] Hexokinase was immobilized on the nano-FET, catalyzing the conversion of adenosine triphosphate (ATP) to adenosine diphosphate (ADP) and causing the phosphorylation of glucose and the release of a proton. This resulted in the protonation of the PPy layer increasing the PPy conductivity to record ATP concentrations near and inside live cells. This concept was further developed to create a nanopipette-based ionic-FET containing one nanoelectrode and one ion channel.[26] A PPy-layer covered the tip of the sensor as the gate electrode. A nanopore acting as a drain source was created in the PPy layer above the ionic channel with an adjustable diameter to match the size of target biomolecules, such as DNA and proteins. By controlling the gate voltage, the charge of the PPy layer was changed and the detection of the translocation events of single, negatively charged DNA molecules was controlled. The embedding of negatively charged insulin in the PPy layer enabled the single molecule detection of IgG antibodies.

The height profile of single cells and the roughness of the surface of tissues are comparable to the size of micrometric SECM tips. As a result the recorded currents are influenced by the topography of the sample. For instance, it can become challenging to discriminate O_2 reduction currents related to cell respiratory activity from those related to the physical blocking of O_2 diffusion. Constant distance mode operations have been achieved, for instance, by combining SECM with SICM (Fig. 1i),[27] shear force distance control[9] or atomic force microscopy (AFM).[28] Contact-mode scanning of delicate and irregular surfaces without feedback control is realized with soft probes made of entirely flexible plastic layers encapsulating a carbon ME.[29] Brushed tissues with strong cellular structures stay intact,[30] but small live cell aggregates will most likely not resist.

Various SPM platforms with electrochemical probes are commercially available, and the tips can either be made relatively easily on site or purchased from various suppliers. The functionalization of the active parts of the probes can require certain expertise. Amperometric electrodes need frequent (electro)chemical cleaning or mechanical polishing due to possible electrode contamination. Soft MEs are refreshed by cutting them with a sharp razor blade.

On-chip detection

Biological specimens can be deposited on flat, nearly two-dimensional chips containing amperometric or potentiometric ME arrays.[34–39] Enzymatic activity is recorded in the generation/collection (G/C) mode, and respiratory activity is recorded in RC mode (Fig. 2a). Read-out times and sensitivity depend on electrical settings, realization of electrode connections and data recording processes. Sequential recording of all electrodes or sub-array units constructs images in microseconds to seconds. A large-scale integration (LSI)-based chip containing 400 Pt or Au MEs with ~107 dpi resolution and a millisecond readout time enabled the correlation of locally induced convective disturbances on the diffusion-limited steady-state currents with the movements of *Daphnia magna* (Fig. 2b).[31] Microchips with 8′192 Pt MEs (~1′150 dpi) were developed to record the microfluidic flows of solutions with different norepinephrine concentrations within 64 s (Fig. 2c).[32] Drawbacks of these array-based systems are usually high production costs caused by clean room environments and expensive material deposition/etching techniques. Electrode fouling can prevent long imaging times and chip reuse. Mechanical polishing of the chip surface would damage the sensing layers, and (electro)chemical cleaning procedures are often not efficient enough. Large tissues can physically block the electrode surface if the samples are not separated from the electrode by using a porous membrane or by using recessed electrodes. Spheroids were placed in a microfluidic hanging drop network under an inverted chip providing a gap between the sample and electrode.[37]

Cells were cultured on carbon-based electrodes, and cellular membrane proteins, labelled with antibodies (Abs) and Ru complexes, were imaged by electrogenerated chemiluminescence (ECL, Fig. 2d).[33] Ultrasensitive single cell imaging assays for cancer diagnostics are envisaged. However, the diffusion length of the electro-generated co-reactant species tri-*n*-propylamine radical ion ($TPrA^{+\bullet}$) and tri-*n*-propylamine radical ($TPrA^{\bullet}$) is limited to 1–2 μm, which is shorter than the

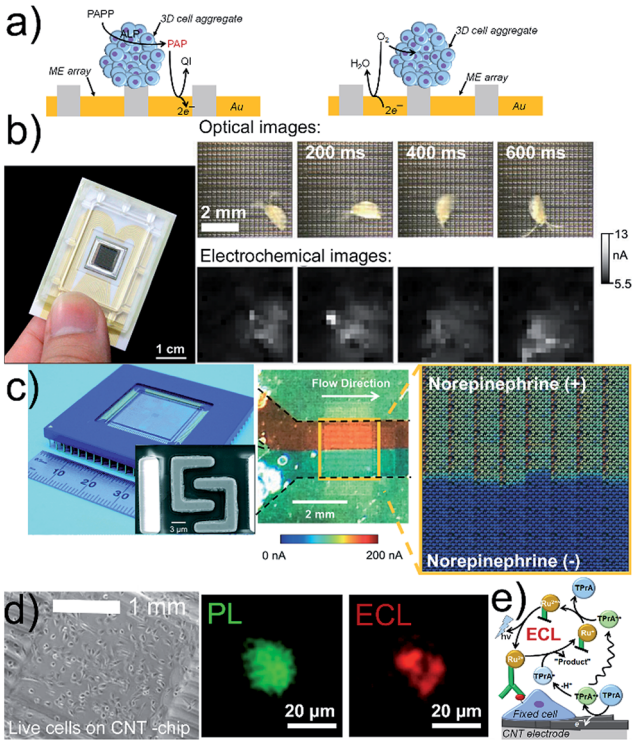

Fig. 2 (a) G/C (left) and RC (right) modes for electrochemical imaging on a chip. (b) 400-ME array chip with an external RE and CE (left) used to track the movement of *Daphnia magna* (right). The oxidation current of $[Fe(CN)_6]^{4-}$ was recorded and perturbed by the motion of *Daphnia magna*. (c) Optical image of a CMOS chip containing 64 subarrays each with 128 Pt MEs and shared RE and CE (left), and SEM image (left, inset) of two interdigitated Pt MEs. Optical image (center) and electrochemical image (right) of a bimodal gradient of two solutions with (+red dye) and without norepinephrine (+blue dye) in neurobasal media. Dashed black lines indicate the walls of a microfluidic channel placed on the chip. Oxidation potential for norepinephrine: +0.6 V *vs.* Pt. (d) Inkjet-printed transparent CNT electrode on plastic with MCF10A cells. Photoluminescence (PL) and ECL images of a MCF10A cell labeled with a cell membrane antibody (Ab) with Ru in 0.2 M phosphate buffer with 200 mM TPrA. Electrode potential: +1.35 V *vs.* Ag/AgCl/KCl 3 M. (e) Scheme of ECL principle. (b) Adapted with permission from ref. 57 (left) and ref. 31 (right). Copyright 2017 American Chemical Society (left) and John Wiley and Sons. (c) Adapted with permission from ref. 32. Copyright 2015 Royal Society of Chemistry. (d) Adapted with permission from ref. 33. Copyright 2017 American Chemical Society.

dimension of a whole cell surface restricting the detection to the portion of the cell-electrode boundary.

Electrochemical imaging of cells

Functional imaging of living cells based on scanning electrochemical probes has become foundational to study cellular mechanisms and their influence in diseases. SECM and SICM offer the opportunity to image cells in viable condition without the use of tagging strategies, which could interfere with and modify the phenomena under study. Imaging cell topographies and their changes can be realized in real time without inducing any stress to the imaged cells.[40–43] The concept of functional imaging is related to the capacity to generate an image reporting the cell functions and is not limited to the mere study of topography. SECM, by employing multiple operation modes, can image the flux of molecules in the proximity of the cell membrane, local chemical reactivity and concentrations, paving the way to the investigation of cell respiration[44,45] and cell metabolism,[46] drug uptake and drug resistance,[47,48] intracellular redox balance and enzymatic reactivity[49,50] and cell membrane permeability, for instance induced by toxic compounds.[51] Several strategies to analyse the respiratory activity of single cells were reported.[44,45] In particular, the importance of preventing O_2 depletion between the cell and the probe, by applying voltage pulse waves, has been highlighted.[52] Combining alternating current (AC) impedance measurements with fast-scan cyclic voltammetry (FSCV) enabled the discrimination of single cell topography from respiratory activity without constant distance operation mode (Fig. 3a).[45]

SICM-SECM constant distance imaging was used to investigate the kinetics and efficiency of cell molecular uptake and delivery at different cell areas (Fig. 3b).[53] It was shown that the uptake at the tip is higher than that at the body of root hair cells. Enzyme-based ME-biosensors were applied to investigate the cell metabolism, *i.e.*, glucose consumption and lactate production (Fig. 3c).[16,46] The intracellular enzymatic activity of cells can be accessed by using cascade reactions with two electroactive species, from which one species penetrates the cell

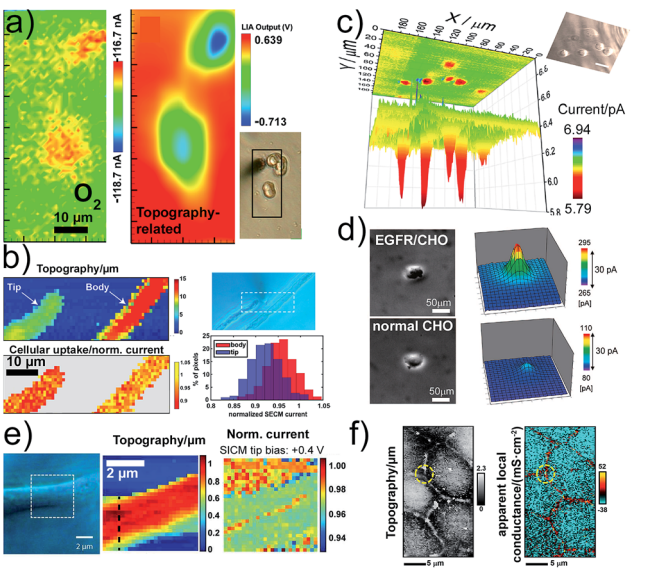

Fig. 3 (a) Electrochemical (FSCV) and topographic (AC-impedance) imaging of PC12 cells. (b) Cellular uptake of $[Ru(NH_3)_6]^{3+}$ as normalized SECM current of single *Zea mays* root hair cells and cell topography. (c) Electrochemical imaging of glucose uptake by single MCF10A cells using a GOx-based Pt-ME-biosensor. (d) Detection of Chinese hamster ovary (CHO) normal cells (upper panels) and transformed EGFR/CHO cells. The ALP/Ab-EGFR-complex was imaged by the electrochemical detection of PAP. (e) SICM mapping of an AbSc cell to detect surface charge heterogeneities on the cell surface. (f) Potentiometric-SICM mapping of the apparent local conductance to identify paracellular and transcellular pathways of ion transport between Madin-Darby Canine Kidney strain II cells. (a–f) Adapted with permissions from ref. 45, 53, 16, 54, 22 and 55. Copyright 2009, 2012, 2016 and 2017 American Chemical Society.

membrane and mediates the regeneration of the other for coupled FB mode imaging.[56] An epidermal growth factor receptor (EGFR), a membrane protein associated with cancer, was imaged in single living cells with SECM by employing Abs labelled with ALP (Fig. 3d).[54] The internal redox balance of cells, which is also associated with cancer transformation, was used to construct electrochemical images with various redox mediators for cancer diagnosis and investigation.[49,50] The use of nanometric pipettes allowed for the highly resolved mapping of charge heterogeneities on the surface of single cells using SICM tip bias-modulation (Fig. 3e).[22] Living human abdominal subcutaneous (AbSc) cells cultured on a positively charged collagen matrix showed a linear positive surface charge region that might be correlated with the location of membrane proteins. Spatially resolved conductance measurements with nanopipettes enabled the visualization of the heterogeneous nanoscale ion transport across junctions between epithelial cells in a cell monolayer (Fig. 3f).[55]

Electrochemical imaging of multicellular structures and tissues

Live multicellular structures and tissues

In reproductive medicine, the selection of best-suited embryos based on non-invasive methods is important for *in vitro* fertilization. The relationship between respiratory activity and the developmental stage of mammalian embryos could be correlated with the long-term development of the embryo by using electrochemical imaging.[58–61] Measurements of the respiratory activity require calibration procedures to determine the oxygen concentration.[62] SECM imaging was used to localize the detectable ALP activity at the surface of mice embryonic stem cell (ESC) spheroids co-cultured with ALP-inactive human breast cancer cells (Fig. 4a).[7] The simultaneous detection of ALP activity and O_2 consumption of embryoid bodies (EBs) was realized with an LSI-chip in dual potential mode (Fig. 4b).[57]

RC-SECM for O_2 reduction of 3D porous tissues containing live hepatocytes and hepatoblastoma cells, grown in polymer- and gelatin-based scaffolds, showed that the hepatocyte activity is mediated by the asialoglycoprotein receptor.[63] This result could be relevant for tissue engineering of the liver for transplantation where the adhesion and proliferation of hepatocytes is an issue. The 3D cell aggregates of live HeLa cells inside microwells were analyzed using RC-SECM for O_2 consumption as a non-invasive live/dead electrochemical assay.[64] Oxygen concentration gradients inside and outside of a live brain slice, excised from mice, were monitored with platinized nanoelectrodes.[11]

One serious threat to human health is an increasing number of bacterial infections related to antimicrobial resistance to antibiotics. Quorum sensing plays an important role and describes a stimuli/response mechanism of bacteria aggregates to monitor their population density and to enhance the transcription of genes when a certain bacterial number is reached during growing. The release of quorum-sensing controlled metabolites, such as electroactive phenazine pyocyanin (PYO),

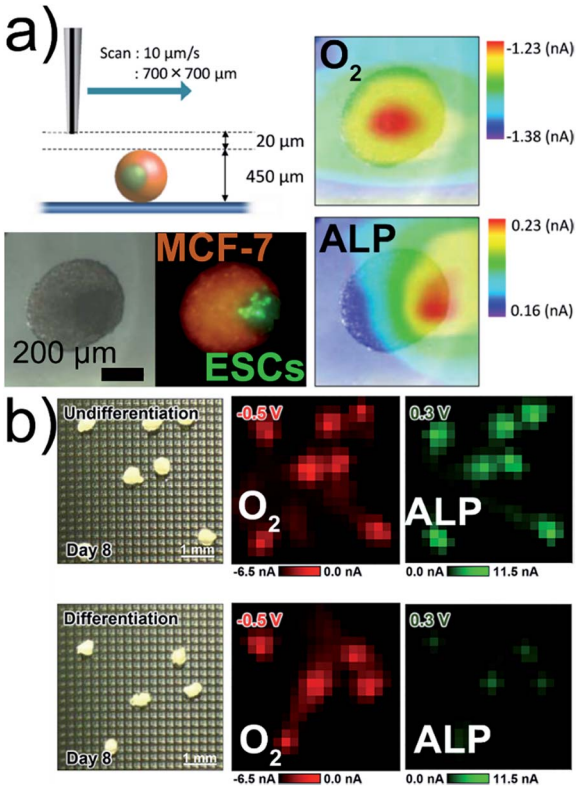

Fig. 4 (a) SECM, optical, and fluorescence imaging of a co-culture Janus spheroid fused on day 3 (250^{ESC}–$2000^{MCF\text{-}7}$). Respiration activity (O_2) imaging at −0.5 V and ALP activity imaging at +0.3 V. (b) Electrochemical imaging of O_2 and ALP activities of EBs. All potentials *vs.* Ag/AgCl. Adapted with permission from ref. 7 and 57. Copyright (a) 2013 and (b) 2017 American Chemical Society.

from *Pseudomonas aeruginosa* aggregates and biofilms were electrochemically imaged.[65–67] SECM imaging revealed that PYO was produced by an aggregate of only 500 cells (Fig. 5a).[65] The chemical communication between two bacteria aggregates, locally separated by 8 µm through a protein-based wall, was confirmed by using two different bacteria strains. One strain (*ΔrhlI*, "responder cells") was able to produce PYO only when *N*-butanoyl-L-homoserine (C_4-HSL), exclusively produced by the other strain (*Δphz*, "producer cells") located in the other well, diffused into the adjacent trap. The chemical communication could be correlated with cell population (>2′000 over an 8 µm distance). Square-wave-voltammetry (SWV) can be applied for multiple metabolite detection where the peaks in the voltammograms at certain potentials can be correlated to different redox active phenazines. This was achieved in less than 7 min by depositing large biofilms, grown on track-etched, agar-soaked membranes, onto a chip with 1′824 MEs.[67] Simultaneous electrochemical imaging of the release of PYO, 5-methylphenazine-1-carboxylic acid (5-MCA) and phenazine-1-carboxylic acid (PCA) was performed, whereas peak currents in the SWVs were converted into concentrations by calibration (Fig. 5b). The production of the phenazines was clearly correlated with certain locations inside the bacterial colony and with oxygenation time.

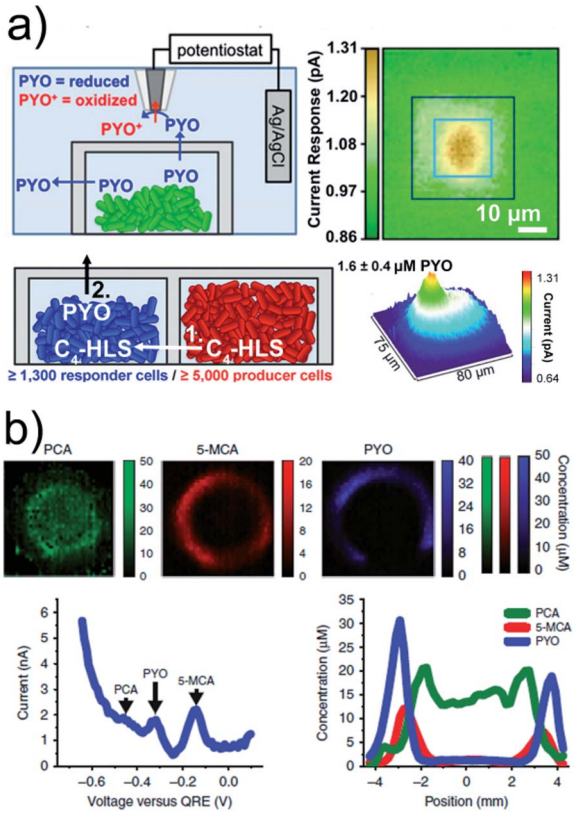

Fig. 5 (a) Upper panels: SECM imaging of PYO (~2.7 µM) release from a *P. aeruginosa* aggregate in a microtrap. The SECM tip was biased at 0 V *vs.* Ag/AgCl to oxidize PYO. Lower panels: PYO was used as a proxy for *P. aeruginosa* QS-controlled communication between physically separated populations using two mutant strains. Aggregates of ≥5000 *Δphz* cells induced PYO production in the neighbouring *ΔrhlI* aggregate. (b) Electrochemical imaging of 2 day anaerobically grown *ΔphzH* biofilms after 4.25 h of oxygenation based on SWV. Phenazine concentration was calculated from the peak currents. Bottom left: exemplary SWV with peak indication. Bottom right: exemplary cross-section from the electrochemical image. (a) Adapted with permission from ref. 65. Copyright 2014 National Academy of Sciences. (b) Adapted from ref. 67. Copyright 2016 Springer Nature.

Large tissue sections

Large tissue samples are characterized by irregular topography. Nanometric SPM tips are suitable for constant distance operation, but impede large area scanning due to long imaging times associated with the small tip size and the required high point density to obtain information, even if scanning speeds have been significantly accelerated.[68,69] Soft linear arrays of eight individual MEs brush over delicate samples like a sensitive comb (Fig. 6a) and were used to image a mouse heart slice (Fig. 6b).[70] The active ME area is not in contact with the sample due to an applied probe angle. Redox-active proteins, such as iron-containing hemoglobin (Hb), which is present in red blood cells, reduced $FcMeOH^+$ allowing FB imaging (Fig. 6c). Finite currents were recorded over the entire tissue and also over redox-inactive parts, most likely due to a diffusion of the redox active species through tissue micropores and accumulation of FcMeOH, a molecule with hydrophobic properties, in certain tissue compartments (Fig. 6d).[70]

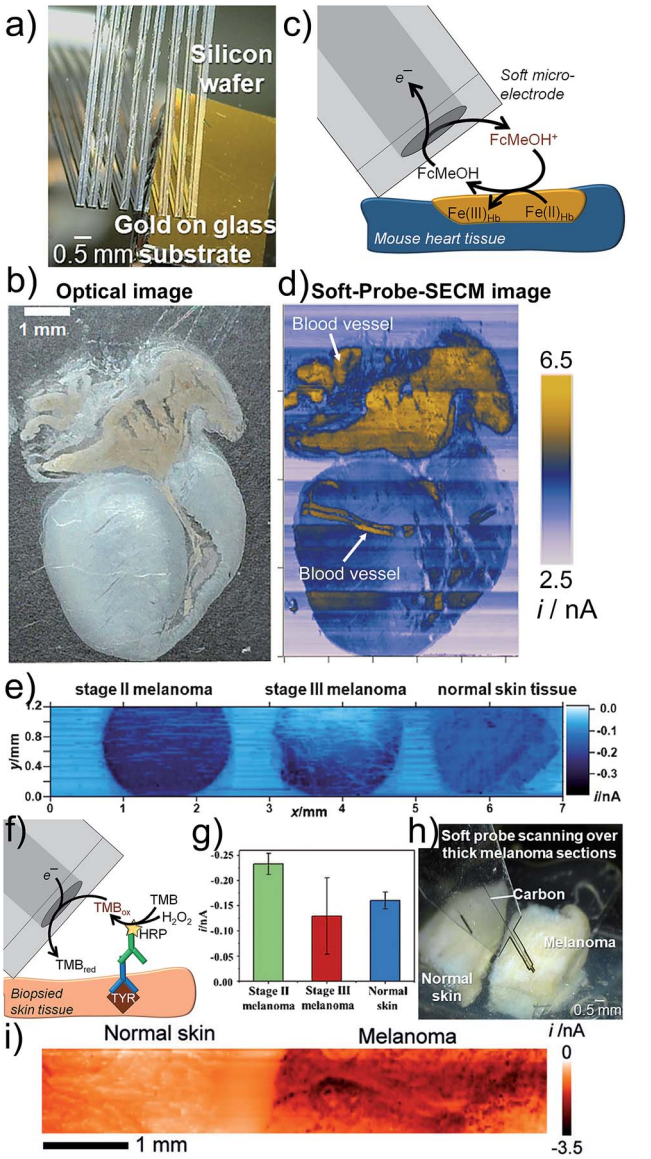

Fig. 6 Soft-Probe-SECM imaging of (a–d) a mouse heart section and (e–i) skin tissue. (a) Soft linear ME array. (b) Optical photograph. (c) FB mode imaging where FcMeOH is regenerated by redox active proteins in the tissue. (d) Soft-Probe-SECM image. (e) Soft-Probe-SECM imaging of the distribution of the diagnostic melanoma biomarker tyrosinase in normal skin and stage II and stage III melanoma slices using an immunoassay-adapted strategy (f). Nine values per tissue were used to create the bar plot in (g). (h and i) Soft-Probe-SECM imaging of thick normal skin and melanoma tissue. Adapted with permission from ref. 70 and 71. Copyright 2016 and 2017 John Wiley and Sons.

Electrochemical imaging of the distribution of the melanoma-associated antigen tyrosinase (TYR) in normal skin, stage II melanoma and stage III melanoma from three different patients was enabled by applying Soft-Probe-SECM to tissue sections (Fig. 6e).[71] An immunoassay against TYR with an HRP label, which catalyses the oxidation of 3,3′,5,5′-tetramethylbenzidine (TMB), was adapted (Fig. 6f). The oxidized species TMB_{ox} was electrochemically reduced at the soft ME. Mechanical sectioning of the tissue broke cell membranes and provided

access to the intracellular components. The SECM image clearly indicates a homogeneous over-expression of TYR in stage II melanoma and a heterogeneous distribution in stage III melanoma. Scanning such large samples with the highest possible resolution, *i.e.* a micrometer step size, takes hours due to the slow probe translation rates required to avoid the convective disturbances of the diffusion of the electroactive species. However, extracting just nine equally distributed data points from each tissue, similar to increasing the probe step size, can reduce the experimental time to seconds and was sufficient to distinguish with high certainty normal skin (moderate TYR concentration, homogeneous), stage II melanoma (TYR over-expressed, homogeneous) and stage III (TYR over-expressed, heterogeneous) by considering the average SECM current (TYR concentration) and error (heterogeneity) (Fig. 6g). Soft MEs are attractive for both thin as well as thick tissue sections (Fig. 6h and i).

Conclusions and perspectives

The use of (sub)micrometer-sized tips, scanned over biological specimens and ME array chips with deposited biological specimens, has demonstrated proficiency in imaging biological functions with micrometer resolution. The large number of sensing units and fast electronics decrease operation times approaching those of optical detection methods. Furthermore, electrochemical imaging can be sensitive and selective. Mass production lowers the prices of devices enabling disposable usage.

Analyzing electrochemical cellular functions in live cells and multicellular structures is important for the understanding of biological processes related to stem cell research, cancer, toxicity, vitality of micro-organisms and antimicrobial resistance. In particular, the broad range of 3D cell culturing methods expands the range of designable experiments and extends the range of electrochemical sensing applications. Combined with "lab-on-a-chip" or "organ-on-a-chip" platforms, electro-chemical imaging can contribute to the replacement of animal experiments. Medical applications, such as the quality control of embryos or skin cancer diagnostics, show great potential. The latter could become attractive if imaging could be applied non-invasively directly on the skin of a patient. Nevertheless, electrochemical imaging is generally limited to superficial events in a tissue. The arrays of electrode spikes could penetrate the upper skin layers, similarly to transdermal drug delivery, for electrochemically imaging the melanoma biomarker distribution inside the epidermis.[72] Electrodes in handheld flexible devices could assist surgeons during an operation with the aim that *in vivo* electrochemical analysis could avoid biopsy. The devices could be combined with 3D printed flexible pens already suitable to extract liquid samples for mass spectrometry,[66,74] as soft microfluidic/-electrodes have already been used for simultaneous SECM-MS imaging.[73] Particularly interesting are the possibilities to affect the microenvironment of live cells for facilitated drug delivery by membrane permeabilization and the electrochemically induced death of cancer cells.

Conflicts of interest

There are no conflicts to declare.

Acknowledgements

S. R. thanks the Associazione Italiana per la Ricerca sul Cancro (AIRC, MFAG 2016 Id.19044).

Notes and references

1 D. Polcari, P. Dauphin-Ducharme and J. Mauzeroll, *Chem. Rev.*, 2016, **116**, 13234–13278.
2 P. K. Hansma, B. Drake, O. Marti, S. A. C. Gould and C. B. Prater, *Science*, 1989, **243**, 641–643.
3 J. Clausmeyer and W. Schuhmann, *Trends Anal. Chem.*, 2016, **79**, 46–59.
4 J. Kwak and A. J. Bard, *Anal. Chem.*, 1989, **61**, 1221–1227.
5 C. Zhao and G. Wittstock, *Angew. Chem., Int. Ed.*, 2004, **43**, 4170–4172.
6 B. R. Horrocks and G. Wittstock, in *Scanning Electrochemical Microscopy*, ed. A. J. Bard and M. V. Mirkin, CRC Press, 2nd edn, 2012, pp. 317–378.
7 T. Arai, T. Nishijo, Y. Matsumae, Y. Zhou, K. Ino, H. Shiku and T. Matsue, *Anal. Chem.*, 2013, **85**, 9647–9654.
8 Y. Zhou, K. Ino, H. Shiku and T. Matsue, *Electrochim. Acta*, 2015, **186**, 449–454.
9 M. Nebel, S. Grützke, N. Diab, A. Schulte and W. Schuhmann, *Angew. Chem., Int. Ed.*, 2013, **52**, 6335–6338.
10 C. Amatore, S. Arbault, M. Guille and F. Lemaître, *Chem. Rev.*, 2008, **108**, 2585–2621.
11 P. Actis, S. Tokar, J. Clausmeyer, B. Babakinejad, S. Mikhaleva, R. Cornut, Y. Takahashi, A. López Córdoba, P. Novak, A. I. Shevchuck, J. A. Dougan, S. G. Kazarian, P. V. Gorelkin, A. S. Erofeev, I. V. Yaminsky, P. R. Unwin, W. Schuhmann, D. Klenerman, D. A. Rusakov, E. V. Sviderskaya and Y. E. Korchev, *ACS Nano*, 2014, **8**, 875–884.
12 Y. Li, K. Hu, Y. Yu, S. A. Rotenberg, C. Amatore and M. V. Mirkin, *J. Am. Chem. Soc.*, 2017, **139**, 13055–13062.
13 S. E. Eklund, D. Taylor, E. Kozlov, A. Prokop and D. E. Cliffel, *Anal. Chem.*, 2004, **76**, 519–527.
14 D. Polcari, A. Kwan, M. R. Van Horn, L. Danis, L. Pollegioni, E. S. Ruthazer and J. Mauzeroll, *Anal. Chem.*, 2014, **86**, 3501–3507.
15 J. P. Wilburn, M. Ciobanu and D. E. Cliffel, *J. Electrochem. Soc.*, 2016, **163**, H3077–H3082.
16 A. Soldà, G. Valenti, M. Marcaccio, M. Giorgio, P. G. Pelicci, F. Paolucci and S. Rapino, *ACS Sens.*, 2017, **2**, 1310–1318.
17 J. G. Ummadi, C. J. Downs, V. S. Joshi, J. L. Ferracane and D. Koley, *Anal. Chem.*, 2016, **88**, 3218–3226.
18 K. McKelvey, B. P. Nadappuram, P. Actis, Y. Takahashi, Y. E. Korchev, T. Matsue, C. Robinson and P. R. Unwin, *Anal. Chem.*, 2013, **85**, 7519–7526.
19 B. P. Nadappuram, K. McKelvey, J. C. Byers, A. G. Güell, A. W. Colburn, R. A. Lazenby and P. R. Unwin, *Anal. Chem.*, 2015, **87**, 3566–3573.

20 A. I. Shevchuk, G. I. Frolenkov, D. Sánchez, P. S. James, N. Freedman, M. J. Lab, R. Jones, D. Klenerman and Y. E. Korchev, *Angew. Chem., Int. Ed.*, 2006, **45**, 2212–2216.
21 P. Novak, C. Li, A. I. Shevchuk, R. Stepanyan, M. Caldwell, S. Hughes, T. G. Smart, J. Gorelik, V. P. Ostanin, M. J. Lab, G. W. J. Moss, G. I. Frolenkov, D. Klenerman and Y. E. Korchev, *Nat. Methods*, 2009, **6**, 279–281.
22 D. Perry, B. Paulose Nadappuram, D. Momotenko, P. D. Voyias, A. Page, G. Tripathi, B. G. Frenguelli and P. R. Unwin, *J. Am. Chem. Soc.*, 2016, **138**, 3152–3160.
23 R. A. S. Nascimento, R. E. Özel, W. H. Mak, M. Mulato, B. Singaram and N. Pourmand, *Nano Lett.*, 2016, **16**, 1194–1200.
24 R. E. Özel, A. Lohith, W. H. Mak and N. Pourmand, *RSC Adv.*, 2015, **5**, 52436–52443.
25 Y. Zhang, J. Clausmeyer, B. Babakinejad, A. López Córdoba, T. Ali, A. Shevchuk, Y. Takahashi, P. Novak, C. Edwards, M. Lab, S. Gopal, C. Chiappini, U. Anand, L. Magnani, R. C. Coombes, J. Gorelik, T. Matsue, W. Schuhmann, D. Klenerman, E. V. Sviderskaya and Y. Korchev, *ACS Nano*, 2016, **10**, 3214–3221.
26 R. Ren, Y. Zhang, B. P. Nadappuram, B. Akpinar, D. Klenerman, A. P. Ivanov, J. B. Edel and Y. Korchev, *Nat. Commun.*, 2017, **8**, 586.
27 Y. Takahashi, A. I. Shevchuk, P. Novak, Y. Murakami, H. Shiku, Y. E. Korchev and T. Matsue, *J. Am. Chem. Soc.*, 2010, **132**, 10118–10126.
28 A. Kueng, C. Kranz, A. Lugstein, E. Bertagnolli and B. Mizaikoff, *Angew. Chem., Int. Ed.*, 2003, **42**, 3238–3240.
29 A. Lesch, B. Vaske, F. Meiners, D. Momotenko, F. Cortés-Salazar, H. H. Girault and G. Wittstock, *Angew. Chem., Int. Ed.*, 2012, **51**, 10413–10416.
30 T. E. Lin, A. Lesch, C. L. Li and H. H. Girault, *J. Electroanal. Chem.*, 2017, **786**, 120–128.
31 K. Ino, Y. Kanno, K. Y. Inoue, A. Suda, R. Kunikata, M. Matsudaira, H. Shiku and T. Matsue, *Angew. Chem., Int. Ed.*, 2017, **56**, 6818–6822.
32 J. B. Wydallis, R. M. Feeny, W. Wilson, T. Kern, T. Chen, S. Tobet, M. M. Reynolds and C. S. Henry, *Lab Chip*, 2015, **15**, 4075–4082.
33 G. Valenti, S. Scarabino, B. Goudeau, A. Lesch, M. Jović, E. Villani, M. Sentic, S. Rapino, S. Arbault, F. Paolucci and N. Sojic, *J. Am. Chem. Soc.*, 2017, **139**, 16830–16837.
34 K. Ino, W. Saito, M. Koide, T. Umemura, H. Shiku and T. Matsue, *Lab Chip*, 2011, **11**, 385–388.
35 K. Ino, T. Nishijo, T. Arai, Y. Kanno, Y. Takahashi, H. Shiku and T. Matsue, *Angew. Chem., Int. Ed.*, 2012, **51**, 6648–6652.
36 J. Rothe, O. Frey, A. Stettler, Y. Chen and A. Hierlemann, *Anal. Chem.*, 2014, **86**, 6425–6432.
37 P. M. Misun, J. Rothe, Y. R. F. Schmid, A. Hierlemann and O. Frey, *Microsyst. Nanoeng.*, 2016, **2**, 16022.
38 K. Ino, M. Şen, H. Shiku and T. Matsue, *Analyst*, 2017, **142**, 4343–4354.
39 Y. N. Lee, K. Okumura, T. Horio, T. Iwata, K. Takahashi, T. Hattori and K. Sawada, *Talanta*, 2018, **179**, 569–574.
40 Y. Takahashi, A. I. Shevchuk, P. Novak, B. Babakinejad, J. Macpherson, P. R. Unwin, H. Shiku, J. Gorelik, D. Klenerman, Y. E. Korchev and T. Matsue, *Proc. Natl. Acad. Sci. U. S. A.*, 2012, **109**, 11540–11545.
41 P. Novak, A. Shevchuk, P. Ruenraroengsak, M. Miragoli, A. J. Thorley, D. Klenerman, M. J. Lab, T. D. Tetley, J. Gorelik and Y. E. Korchev, *Nano Lett.*, 2014, **14**, 1202–1207.
42 F. Razzaghi, J. Seguin, A. Amar, S. Griveau and F. Bedioui, *Electrochim. Acta*, 2015, **157**, 95–100.
43 M. S. M. Li, F. P. Filice and Z. Ding, *J. Electroanal. Chem.*, 2016, **779**, 176–186.
44 X. Zhao, P. M. Diakowski and Z. Ding, *Anal. Chem.*, 2010, **82**, 8371–8373.
45 J. A. Koch, M. B. Baur, E. L. Woodall and J. E. Baur, *Anal. Chem.*, 2012, **84**, 9537–9543.
46 M. Ciobanu, D. E. Taylor Jr, J. P. Wilburn and D. E. Cliffel, *Anal. Chem.*, 2008, **80**, 2717–2727.
47 D. Koley and A. J. Bard, *Proc. Natl. Acad. Sci. U. S. A.*, 2012, **109**, 11522–11527.
48 S. Kuss, R. Cornut, I. Beaulieu, M. A. Mezour, B. Annabi and J. Mauzeroll, *Bioelectrochemistry*, 2011, **82**, 29–37.
49 S. Rapino, R. Marcu, A. Bigi, A. Soldà, M. Marcaccio, F. Paolucci, P. G. Pelicci and M. Giorgio, *Electrochim. Acta*, 2015, **179**, 65–73.
50 B. Liu, S. A. Rotenberg and M. V. Mirkin, *Proc. Natl. Acad. Sci. U. S. A.*, 2000, **97**, 9855–9860.
51 M. S. M. Li, F. P. Filice, J. D. Henderson and Z. Ding, *J. Phys. Chem. C*, 2016, **120**, 6094–6103.
52 M. Nebel, S. Grützke, N. Diab, A. Schulte and W. Schuhmann, *Faraday Discuss.*, 2013, **164**, 19–32.
53 A. Page, M. Kang, A. Armitstead, D. Perry and P. R. Unwin, *Anal. Chem.*, 2017, **89**, 3021–3028.
54 Y. Takahashi, T. Miyamoto, H. Shiku, R. Asano, T. Yasukawa, I. Kumagai and T. Matsue, *Anal. Chem.*, 2009, **81**, 2785–2790.
55 L. Zhou, Y. Gong, J. Hou and L. A. Baker, *Anal. Chem.*, 2017, **89**, 13603–13609.
56 Y. Matsumae, Y. Takahashi, K. Ino, H. Shiku and T. Matsue, *Anal. Chim. Acta*, 2014, **842**, 20–26.
57 Y. Kanno, K. Ino, H. Abe, C. Sakamoto, T. Onodera, K. Y. Inoue, A. Suda, R. Kunikata, M. Matsudaira, H. Shiku and T. Matsue, *Anal. Chem.*, 2017, **89**, 12778–12786.
58 H. Shiku, T. Shiraishi, H. Ohya, T. Matsue, H. Abe, H. Hoshi and M. Kobayashi, *Anal. Chem.*, 2001, **73**, 3751–3758.
59 Y. Date, S. Takano, H. Shiku, K. Ino, T. Ito-Sasaki, M. Yokoo, H. Abe and T. Matsue, *Biosens. Bioelectron.*, 2011, **30**, 100–106.
60 K. Hiramoto, M. Yasumi, H. Ushio, A. Shunori, K. Ino, H. Shiku and T. Matsue, *Anal. Chem.*, 2017, **89**, 10303–10310.
61 M. Şen, K. Ino, K. Y. Inoue, T. Arai, T. Nishijo, A. Suda, R. Kunikata, H. Shiku and T. Matsue, *Biosens. Bioelectron.*, 2013, **48**, 12–18.
62 H. Kurosawa, H. Utsunomiya, N. Shiga, A. Takahashi, M. Ihara, M. Ishibashi, M. Nishimoto, Z. Watanabe, H. Abe, J. Kumagai, Y. Terada, H. Igarashi, T. Takahashi, A. Fukui, R. Suganuma, M. Tachibana and N. Yaegashi, *Hum. Reprod.*, 2016, **31**, 2321–2330.
63 K. S. Vasanthan, S. Sethuraman and M. Parthasarathy, *Anal. Chim. Acta*, 2015, **890**, 83–90.

64 A. Sridhar, H. L. De Boer, A. Van Den Berg and S. L. Gac, *PLoS One*, 2014, **9**, e93618.
65 J. L. Connell, J. Kim, J. B. Shear, A. J. Bard and M. Whiteley, *Proc. Natl. Acad. Sci. U. S. A.*, 2014, **111**, 18255–18260.
66 D. Koley, M. M. Ramsey, A. J. Bard and M. Whiteley, *Proc. Natl. Acad. Sci. U. S. A.*, 2011, **108**, 19996–20001.
67 D. L. Bellin, H. Sakhtah, Y. Zhang, A. Price-Whelan, L. E. P. Dietrich and K. L. Shepard, *Nat. Commun.*, 2016, **7**, 10535.
68 H. Ida, Y. Takahashi, A. Kumatani, H. Shiku and T. Matsue, *Anal. Chem.*, 2017, **89**, 6015–6020.
69 D. Momotenko, J. C. Byers, K. McKelvey, M. Kang and P. R. Unwin, *ACS Nano*, 2015, **9**, 8942–8952.
70 T. E. Lin, Y. J. Lu, C. L. Sun, H. Pick, J. P. Chen, A. Lesch and H. H. Girault, *Angew. Chem., Int. Ed.*, 2017, **56**, 16498–16502.
71 T. E. Lin, A. Bondarenko, A. Lesch, H. Pick, F. Cortés-Salazar and H. H. Girault, *Angew. Chem., Int. Ed.*, 2016, **55**, 3813–3816.
72 B. Ciui, A. Martin, R. K. Mishra, B. Brunetti, T. Nakagawa, T. J. Dawkins, M. Lyu, C. Cristea, R. Sandulescu and J. Wang, *Adv. Healthcare Mater.*, 2018, DOI: 10.1002/adhm.201701264.
73 A. Bondarenko, F. Cortés-Salazar, M. Gheorghiu, S. Gáspár, D. Momotenko, L. Stanica, A. Lesch, E. Gheorghiu and H. H. Girault, *Anal. Chem.*, 2015, **87**, 4479–4486.
74 J. Zhang, J. Rector, J. Q. Lin, J. H. Young, M. Sans, N. Katta, N. Giese, W. Yu, C. Nagi, J. Suliburk, J. Liu, A. Bensussan, R. J. Dehoog, K. Y. Garza, B. Ludolph, A. G. Sorace, A. Syed, A. Zahedivash, T. E. Milner and L. S. Eberlin, *Sci. Transl. Med.*, 2017, **9**, eaan3968.